Title

A benchmark fracture mechanics solution for a two-dimensional eigenstrain problem considering residual stress, the stress intensity factor, and superposition

Authors

Ribeiro, Renan L
Hill, Michael R

Publication Date

2016-09-01

DOI

10.1016/j.engfracmech.2016.06.007

Peer reviewed

A benchmark fracture mechanics solution for a two-dimensional eigenstrain problem considering residual stress, the stress intensity factor, and superposition

Renan L. Ribeiro
Michael R. Hill*

Department of Mechanical and Aerospace Engineering,
University of California, One Shields Avenue, Davis, CA 95616 United States

Submitted to Engineering Fracture Mechanics January, 2016

ABSTRACT

Eigenstrain is a distributed strain field considered in mechanics that is particularly helpful in evaluating residual stress fields in the finite element method, and estimating the stress intensity factor due to residual stress in cracked components. The objective of this paper is to provide a solution for a simple eigenstrain problem in a two-dimensional rectangular domain that can serve as a benchmark for validation of fracture mechanics analysis methods. The solution provides residual stress fields and the stress intensity factor for a single edge crack as a function of crack size. Documenting the benchmark provides opportunities to demonstrate the correlation of different means to determine the stress intensity factor and to highlight details in implementing stress intensity factor calculations.

Keywords: Eigenstrain, residual stress, finite element analysis, stress intensity factor, weight function

1. INTRODUCTION

Residual stresses are known to have an important influence on fatigue life [1]. Significant research efforts have been devoted to prediction of residual stresses from processes that enhance fatigue performance of materials by introducing compressive residual stresses [2–4]. One of the leading methods to analyze residual stresses is the eigenstrain method [5], which reconstructs the complete residual stress field based on an elastic finite element analysis that includes the initial permanent strain (i.e., the eigenstrain field) causing the residual stress. The eigenstrain field is determined using process modeling or experimental measurements. Because fatigue failure

* Corresponding author. Tel.: 530-754-6178; fax: 530-752-4158.
E-mail address: mrhill@ucdavis.edu

comprises the initiation and propagation of cracks, the stress intensity factor of fracture mechanics (and the related J-integral) is important in fatigue life prediction.

Calculation of the stress intensity factor is a conventional technology, but care is required when assessing the combined effects of applied loads and residual stresses. Stress intensity factors for applied loads are typically computed using available handbook solutions for simple cases, or using finite element or boundary element methods for complex cases. For residual stresses, stress intensity factors can be determined using the weight function method for simple cases, or the more general finite element or boundary element methods for complex cases. The principle of superposition is typically used to combine the effects of residual stresses and cyclic applied loads when assessing fatigue and fracture behavior.

1.1 The eigenstrain method

The term eigenstrain was initially suggested by Mura [6], and eigenstrain methods have been discussed by several authors in the context of assessing residual stress fields. According to DeWald and Hill [7], eigenstrain can be considered an inelastic strain distribution that causes a given residual stress field. It is an incompatible strain field that does not satisfy geometric (strain) compatibility, and leads to a total strain field that satisfies mechanical equilibrium through an induced residual stress field. A previous study demonstrates the use of eigenstrain methods to simplify the estimation of stress fields from compressive residual stress surface treatments [7,8]. In that work, a simplified eigenstrain field was determined from limited residual stress measurement data, and finite element models where used to determine the full residual stress field from the eigenstrain. Coratella et al. [9] provide a recent validation of that earlier work in aerospace aluminum alloy (7050-T7451) samples with residual stresses from laser shock peening (LSP). Luckhood, Jun, and Korsunsky [10] have used the eigenstrain method to analyze

residual stresses measured in friction stir welds. Kartal et al. [11] illustrate the use of eigenstrain for determination of microscale residual stresses near an inclusion in a nickel alloy. A closely related approach is to use non-linear process models, rather than measurements, to approximate the eigenstrain field produced by a given process. For example, Achintha and Nowell [12], and Hu and Grandhi [13], have used non-linear (finite element) process models for LSP to determine the stabilized plastic strain fields imparted by LSP in simple geometries, and then used the plastic strain fields as input to an eigenstrain analysis to predict residual stress fields from LSP in parts with complex geometry. While the process models are time-consuming, and the residual stress fields they determine are specific to the geometry assessed in the process model, the eigenstrain analysis is linear, which allows complex geometries and large parts to be assessed rapidly. While the literature has a number of publications describing eigenstrain methods, there is a lack of published work on the use of eigenstrain analysis to assess the role of residual stress in fracture mechanics calculations.

1.2 The weight function method

Stress intensity factors for residual stresses and applied loads are determined using the principles of solid mechanics. The weight function method is a powerful technique that allows the stress intensity factor in a specific geometry to be found for a known, but arbitrary, stress distribution acting to open (considering Mode I) the crack. The weight function method has been discussed extensively in the literature, having been initially envisioned by Bueckner [14] and summarized in the more recent book by Wu and Carlsson [15]. There are analytical weight function expressions available that allow for stress intensity factor determinations in a variety of simple geometries (such as panels with center or edge cracks, and cracks at holes). The initial work by Bueckner [14], and subsequent works by Rice [16], Paris et al [17], and Parker and

Bowie [18] show that the stress intensity factor due to an arbitrary loading can be determined by an integration over the crack length of the product of the weight function and the stress field acting to open the crack. The method applies whether the stress field is due to applied loads, residual stress, or their combination. Considering an edge crack, the stress intensity factor K as a function of crack length a is found from

$$K(a) = \int_0^a \sigma(x) m(a,x) dx \tag{1}$$

where x is a coordinate along the crack line, with origin at the crack mouth, $\sigma(x)$ is the stress acting at the crack line, and $m(a, x)$ is a weight function.

Several authors have published weight functions that enable stress intensity factor calculations for a range of geometry and crack type. Wu and Carlsson [15] provided weight functions for several one-dimensional (edge or middle) crack configurations in two-dimensional bodies, and offer valuable supporting technical background regarding weight function methods. Shen and Glinka [19] studied weight functions for stress intensity factor calculations in surface semi-elliptical cracks in finite thickness plates. They validated their expressions against stress intensity factors determined using finite element methods, assuming bending (linear), quadratic, and cubic variations of stress with depth from the plate surface. The validations showed that the weight function provided reasonable stress intensity factor accuracy for the various stress fields, with differences from finite element results of less than 5% for a range of crack depths ($0 \leq a/t \leq 0.8$) and crack aspect ratio ($0.2 \leq a/c \leq 1$), where a is the crack depth, t is the plate thickness, and $2c$ is the crack surface length. Zheng et al. [20] did similar work, developing weight functions for surface semi-elliptical cracks on the inner diameter of a thick-walled cylinder, and validating their results against stress intensity factors from finite element data.

The objective of this paper is to provide a benchmark solution including the residual stress and the stress intensity factor for an edge cracked plate containing a known eigenstrain field. The solution uses the finite element method, and assumes two-dimensional plane stress. The given eigenstrain field is imposed using an isotropic thermal strain, and crack propagation is simulated by releasing nodes along the crack line. A second finite element model is developed using the principle of superposition of crack face tractions to demonstrate its validity and equivalence for the stress intensity factor calculation. In addition, we assess the performance of the weight function method for the numerical calculation of the stress intensity factor in this particular scenario relative to the results from the finite element method. The reference solution here should serve as a useful reference point when validating fracture mechanics calculations for residual stress bearing bodies.

2. METHODS

2.1 Problem description

We consider the geometry and loading in Figure 1a. The problem domain consists of a thin plate in two-dimensional space, having width W = 1 and height H = 2W. A central square area of side 0.5W contains a known equibiaxial eigenstrain field ε^*, given by

$$\varepsilon^* = \begin{Bmatrix} \varepsilon^*_{xx} \\ \varepsilon^*_{yy} \\ \varepsilon^*_{xy} \end{Bmatrix} = \begin{Bmatrix} 0.001 \\ 0.001 \\ 0.000 \end{Bmatrix} \tag{2}$$

where the asterisk denotes an eigenstrain field, as suggested by Mura [6]. This field is a simplification of one described in earlier work [21] that was induced by applying LSP to a thin plate, in a small square region. Measurements of residual stress, and interesting results of fatigue and fracture tests presented in [22] provided motivation for using this eigenstrain field in the present work. The coordinate system shown in Figure 1a has its origin at the left edge of the

plate at mid height. The plate has an edge crack of size a. The key elements of the problem are to find the stress in the uncracked plate, and then to determine the stress intensity factor (SIF) for cracks of size $a/W \leq 0.9$.

2.2 Problem solution by a finite element model

Finite element simulations are carried out using a commercial code [23]. The eigenstrain field is applied through the use of an isotropic thermal strain. Only half the structure was modeled using one symmetry boundary condition because the geometry and loading are symmetric. The right lower corner node was constrained in the x direction to prevent rigid body motion. The half model with the boundary conditions and the area of application of the eigenstrain field is shown in Figure 1b. Two different materials (with the same elastic properties, but different thermal expansion coefficients) were used in the model to apply the eigenstrain field. A material having thermal expansion coefficients equal to zero is defined for the plate, excluding the square area that contains the eigenstrain field. The material in the central square area has thermal expansion coefficients equivalent to the eigenstrain of Eq. (2). Both materials are elastic with modulus of elasticity $E = 1$, and Poisson ratio 0.3. A unit temperature increase in the whole model results in the appropriate eigenstrain field. The edge crack was introduced by changing the nodes restrained on the crack plane, with nodes unrestrained for $x < a$ and restrained for $x \geq a$. The SIF is determined by the commercial code using the domain integral technique, which is described below.

The J-integral is a well-accepted fracture mechanics parameter related to the energy release associated with crack growth. It is a measure of the intensity of deformation at a notch or crack tip, and it is related to the stress intensity factors if the material response is linear [24]. As

described in the commercial code documentation, the J-integral is defined in two dimensions (in the context of quasi-static analysis) as

$$\mathrm{J} = \lim_{\Gamma \to 0} \int_{\Gamma} \boldsymbol{n} \cdot \boldsymbol{H} \cdot \boldsymbol{q} d\Gamma, \tag{3}$$

where Γ is a contour beginning on the bottom crack surface and ending on the top surface, as shown in Figure 2a. The vector **q** is a unit vector in the virtual crack extension direction, and **n** is the outward normal to Γ. H is a second order tensor given (in index notation) by

$$H_{ij} = U\delta_{ij} - \sigma_{ik} \frac{\partial u_k}{\partial x_j} \tag{4}$$

where U is the elastic strain energy density for elastic materials (for elastic-plastic or elastic viscoplastic material behavior, U is defined as the elastic strain energy density plus the plastic dissipation), δ_{ij} is the Kronecker-delta, σ is the stress tensor, and u is the displacement vector. Using the divergence theorem, the contour (line) integral can be converted into a domain (area) integral, given by

$$J = -\int_{A} \left(\frac{\partial}{\partial \boldsymbol{x}}\right) \cdot (\boldsymbol{H} \cdot \overline{\boldsymbol{q}}) d\Gamma - \int_{C_+ + C_-} \boldsymbol{t} \cdot \frac{\partial \boldsymbol{u}}{\partial \boldsymbol{x}} \cdot \overline{\boldsymbol{q}} d\Gamma \tag{5}$$

where $\mathbf{t} = \mathbf{m} \,.\, \boldsymbol{\sigma}$ is the surface traction on the crack surfaces C_+ and C_-, **m** is the outward normal to the domain enclosed by the closed contour $C + C_+ + \Gamma + C_-$, and $\overline{\boldsymbol{q}}$ is a sufficiently smooth weighting function within the region enclosed by the same closed contour. These parameters are shown in Figure 2b. The domains are defined in the commercial code as rings/layers of elements surrounding the crack tip. The first domain consists of elements directly connected to the crack-tip nodes. The subsequent domain adds the ring of elements that share nodes with the elements from the first domain. Following this scheme, each subsequent domain includes the prior domain

and the next ring of elements that share nodes with the elements in the previous domain. Typically, the J-integral is evaluated on a number of domains, and valid results are independent of domain except for very small domains, which are prone to error, or large domains that may be influenced by far field boundaries [24].

The stress intensity factors K_I, K_{II}, and K_{III} are related to the J-integral through

$$J = \frac{1}{8\pi} \boldsymbol{K^T} \cdot \boldsymbol{B^{-1}} \cdot \boldsymbol{K} \tag{6}$$

where $\mathbf{K} = [K_I \ K_{II} \ K_{III}]^T$ are the stress intensity factors and **B** is a pre-logarithmic energy factor matrix. This equation is simplified for homogeneous isotropic materials, and becomes

$$J = \frac{1}{\bar{E}} \left({K_I}^2 + {K_{II}}^2 \right) + \frac{1}{2G} {K_{III}}^2 \tag{7}$$

where $\bar{E} = E$ for plane stress and $\bar{E} = E/(1 - v^2)$ for plane strain. In this model, the SIF (K_I) was determined as an output of the commercial code, being calculated through the use of the domain integral.

It is important to recognize that previous research has shown that the presence of residual stresses and eigenstrain in a body can lead to erroneous path dependence of the domain integral [25]. In this case, further care is needed to determine a single value of J from the results obtained on various domains (e.g., often ad hoc schemes). Lei et al. [26] presented a methodology to provide domain-independent values of the domain integral in two-dimensional bodies with the presence of residual stresses. This methodology was further extended to three-dimensional modeling by Meith and Hill [27]. In the current work, the domain integral was computed using the built-in capabilities of the commercial code [23], and the domain dependence of the SIF was explored by computing the domain integral of 15 domains.

The finite element mesh had two-dimensional, eight-node biquadratic, plane stress quadrilateral elements. The elements at the crack line were square and uniform, with side length equal to 0.0025W, which provided a highly refined mesh along the crack line. This degree of mesh refinement was sufficient to ensure that values of the SIF were converged to better than 0.5%. A first step in the analysis determined the stress field in the uncracked body. In subsequent steps, 72 crack sizes were studied, starting from a/W = 0.0125 and increasing in increments of 0.0125 up to a/W = 0.9. The crack sizes a/W = 0.25 and a/W = 0.75 have the crack tip exactly on the interface between different materials.

2.3 Superposition principle

For linear elastic materials, the stress intensity factors are additive for the same mode of loading [28], on account of the principle of superposition. This principle can be useful for calculating stress intensity factors for complex configurations, since the solution can be built by superposing simple cases for which solutions might be available and well established in the literature. For the particular problem in this study, the principle of superposition can be used to confirm the results obtained from the finite element model with the eigenstrain input. One way of applying this principle to the current problem is shown in Figure 3, which is similar to figures in the early literature on fracture mechanics [14,17]. Figure 3a shows the plate with the eigenstrain field, but with no crack. The stress intensity factor for this case is readily known to be zero. Figure 3b shows the configuration described in section 2.1, containing the eigenstrain field and an edge crack. In the uncracked body, the eigenstrain causes a normal stress field, σ_{yy} at the crack line (y = 0). If this resulting stress profile is applied at the crack line in the configuration shown in Figure 3c, then the stress intensity factor will be the same as in the eigenstrain bearing body, according to the principle of superposition. In other words, applying the stress profile from

configuration (a) at the crack faces in configuration (c) has the same effect as applying the eigenstrain field for the stress intensity factor calculation. A finite element model for the configuration in Figure 3c was created using the same mesh used for the eigenstrain model, but using no thermal strain. The stress profile was applied at the crack faces as a distributed pressure, and the resulting stress intensity factor was evaluated for the range of crack sizes. This allows verification of the stress intensity factor calculations for cases of distributed strain and crack face tractions, both of which require special techniques for domain integral calculations [29].

2.4 The weight function method for stress intensity factor calculation

The weight function method described by Wu and Carlsson [15] was used to calculate the stress intensity factor for the geometry and loading considered in this paper. This method has a remarkable computational efficiency without compromising solution accuracy. One of the inputs to the weight function method is the stress field along the crack line in the uncracked plate. This stress field is obtained from the finite element model of the uncracked body. The other input required is the crack size of interest.

The weight function corresponds to a single edge crack in a finite width plate, as shown in Figure 4. We use the expression from Wu and Carlsson [30]

$$m(a,x) = \frac{1}{\sqrt{2\pi a}} \sum_{i=1}^{5} \beta_i(a) \,.\, (1 - \frac{x}{a})^{i-\frac{3}{2}} \tag{8}$$

which is a function of the crack size a, and the coordinate along the crack line x. The parameters β_i (i = 1,2,3,4,5) are functions of the normalized crack size, a/W, and Table 1 provides summary values of β_i for a range of crack size, which were computed according to [30].

The stress intensity factor for an arbitrary crack face loading is calculated using Eq. (1). From the finite element model, the crack line stress at the nodes is available as a set of data

points. For a desired crack size, the weight function can be determined (using Eq. (8)) as a function of the coordinate x, given the values of β_i. The SIF for the desired crack size is then determined by numerical integration using adaptive Gauss-Kronrod quadrature [31]. The quadrature is useful given the expected discontinuous behavior of the stress field along the crack line in the uncracked body, and the singularity of m(x,a) as x approaches a.

3. RESULTS

3.1 Results from the eigenstrain FE model

The stress profile along the crack line (y = 0) from the eigenstrain model of the uncracked body is shown in Figure 5. This stress profile serves as an input for the calculation of the stress intensity factor using the weight function method, along with the desired crack sizes. The same stress profile was also used in the equivalent finite element model of Figure 3c, as a traction field applied to the crack face.

Stress intensity factor results from the eigenstrain model for representative crack sizes are shown in Figure 6 as a function of the domain size. The stress intensity factor values are normalized by $S\ W^{0.5}$, where S = 0.001E (where 0.001 is the maximum value of the eigenstrain field), which scales the stress field. The normalized stress intensity factor is expected to reach a plateau with domain size when the domain integral calculation is correct, so that the SIF is domain independent. Figure 6 shows the results for crack sizes in the plate material up to a/W = 0.25 (first discontinuity) and one crack size in the eigenstrain area, a/W = 0.275. For a crack size of a/W = 0.1, the SIF is domain independent, and a useful SIF is determined. For a/W = 0.25, the crack tip is at the eigenstrain discontinuity, the SIF is domain dependent, and the values are not useful. For this crack size, the contour integral domain always includes the discontinuity. For the

crack sizes close to the discontinuity (a/W = 0.225 and 0.275), the SIF is domain independent until the domain includes the discontinuity. The same trend was observed for longer crack sizes, near the second discontinuity (a/W ≈ 0.75).

The normalized SIF as a function of a/W for the eigenstrain FE model is shown in Figure 7 (along with the results from the weight function and the equivalent FE model (Figure 3c) that are discussed below). The dashed line is broken around the discontinuity points (a/W = 0.25 and 0.75) because of the lack of data due to the domain dependence of the SIF. The SIF increases monotonically up to a crack size of a/W = 0.25, which corresponds to the first discontinuity in the stress profile. After the discontinuity, the normalized SIF decreases monotonically until the crack reaches the second discontinuity in the stress field. After this point, the normalized SIF increases and approaches zero as a/W approaches unity. The characteristics of the SIF trend with crack size are reasonable given the mathematical (integral) relationship between the SIF and the stress field (Eq. (1)).

3.2 Results from the equivalent FE model

Stress intensity factor results versus domain size from the equivalent FE model (Figure 3c) are shown in Figure 8 for the same crack sizes as in Figure 6 for the eigenstrain model. The SIF values for the equivalent model are domain independent for all crack sizes.

The normalized SIF as a function of crack size obtained from the equivalent FE model is compared to the SIF from the eigenstrain FE model in Figure 7. The results from both FE models have a very good agreement for all crack sizes, which demonstrates the validity of superposition. The equivalent model provides good SIF values at all crack sizes, particularly near the discontinuity.

3.3 Results from the weight function method

The SIF calculated from the weight function method as a function of crack size is shown with results from the finite element models in Figure 7. The weight function and finite element results are very similar, having discontinuities in slope at the same points as the stress profile discontinuities (a/W = 0.25 and 0.75). For longer crack sizes, a/W > 0.7, the difference between the SIF from the FE models and the weight function increases significantly. Figure 9 shows the relative difference of the SIF results from the equivalent model and weight function relative to the eigenstrain model results (benchmark FE model). This model represents the benchmark since the stress resultant from this model is used as an input in the equivalent model and also the weight function approach. The relative difference between the weight function and eigenstrain FE model is very small up to a/W = 0.25, and increases after each discontinuity point, but remains under 2% for a/W < 0.7 and is less than 4.2% for the whole range of crack size. Errors in the weight function SIF values are larger for large cracks (a/W > 0.75), and this is discussed below.

4. DISCUSSION

According to release notes for the commercial code [32], as of 2011 the code includes the effect of residual stress fields in contour integral evaluation, so as to provide domain independent contour integral values. However, as illustrated here, the software does not provide domain independent values of the SIF when the domain includes a discontinuity in material property (i.e., thermal expansion coefficients). An alternative way to model the current eigenstrain problem is by using continuous material properties throughout the whole rectangular domain (i.e., single material with appropriate thermal expansion coefficients), but discontinuous temperature (i.e., T = 1 in the area of non-zero eigenstrain, T = 0 elsewhere). This provides

nearly the same eigenstrain distribution (excepting a small effect that arises because a sharp discontinuity in temperature cannot be expressed exactly, since nodal temperature gradients are limited by node spacing). This alternate eigenstrain model was evaluated using the same mesh and crack sizes as before, and domain independent values of the SIF were observed for all crack sizes. The results are shown in Figure 10, and agree with the previous results obtained from the eigenstrain FE model and the equivalent FE model. When the crack tip is at the first discontinuity, a/W = 0.25, the new SIF is somewhat lower than the value obtained from the equivalent model, but when the crack tip is at the second discontinuity, a/W = 0.75, the two models give nearly identical results. The difference in SIF for two identical eigenstrain fields, one with spatially varying temperature and the other with spatially varying thermal expansion coefficient, is unexpected (and undocumented) and potentially problematic for a typical user.

The discontinuities in the stress field at x/W = 0.25 and 0.75 in Figure 5 were expected because of the discontinuities in the eigenstrain input. The applied eigenstrain field produces compressive residual stresses in the central square area. Outside this area, tensile stresses develop to provide for mechanical equilibrium. This is a result from the deformation of the surrounding material to accommodate the eigenstrain. It is important to recognize that the stress field shown in Figure 5 is the total residual stress (σ_{TOT}), which can be considered as a superposition of the stress due to the eigenstrain only (σ^*), and the residual stress arising to satisfy equilibrium (σ_{EQ}) [7]. This relationship can be expressed as

$$\sigma_{TOT} = \sigma^* + \sigma_{EQ} \tag{9}$$

The stress σ^* can be calculated using the stress-strain relationship $\sigma^* = -E\varepsilon^*$. Figure 11 shows the yy component of stress separated using Eq. (9). The stress from eigenstrain σ^* is zero outside the central square area, and constant inside it, due to the discontinuous behavior of the

eigenstrain. The stress arising to satisfy equilibrium (σ_{EQ}) is continuous and nearly constant with position across the plate. The concept of the superposition of the stress is very useful when deriving eigenstrains from a particular residual stress distribution, as discussed by DeWald and Hill [7].

It is interesting to discuss the choice of the configurations in Figure 3 used for the principle of superposition. Anderson [28] shows an example of a semielliptical surface crack under constant internal pressure *p*. For that case, it is shown that having *p* acting on the crack face is equivalent (with respect to the SIF) to having *p* acting on the boundary, according to the superposition principle. In other words, crack-face tractions can be replaced by boundary tractions, and vice versa, such that the SIF stays the same. However, it is important to recognize that this is true for a constant stress, but not for a more complex stress profile. In this paper, the stress profile generated at the crack line due to the eigenstrain field is a self-equilibrating stress, and its resultant is zero (i.e., integrating the stress on the cross section results in zero). Because of this, crack face tractions are used in Figure 3c, instead of applying the tractions at the boundary. If boundary tractions were used, the stress at the crack line would be close to zero, according to St Venant's principle, and the SIF would also be nearly zero. To further consider this issue, consider the rectangular domain of Figure 1b with a discontinuous boundary traction at the top (y = 1) that has a value of 0.001E for $x < 0.1W$, and 0 for $x \geq 0.1W$. Figure 12 shows the applied boundary traction, along with the resulting stress at the crack line obtained from a finite element model. Both stress profiles provide the same resultant force, but are fundamentally different. Introducing an edge crack of size a/W = 0.1 and calculating the normalized SIF (in the same manner as described before) results in 2.2729E-01. Working the contrary problem, applying the same discontinuous traction on the crack face, and then computing the normalized

SIF results in 6.5597E-01. The difference between the two SIFs is very large, about 65%, which reinforces the notion that crack line stresses must be used to produce accurate SIF results.

The weight function method is known to become unstable for long cracks, and this becomes clear for normalized crack sizes greater than 0.75 in Figure 7 where the error in stress intensity factor increases. Wu and Carlsson [30] show the stress intensity factor results for a rectangular plate with a self-equilibrating fourth power stress at the crack line, and the accuracy is estimated to be better than 1% for $a/W < 0.6$. For a bending stress distribution and parabolic stress distribution, the accuracy was estimated to be better than 1% for $a/W < 0.8$. For a plate subjected to residual stress due to plastic bending at limit load, the accuracy was 1% up to $a/W < 0.5$. But, for all of these examples, the accuracy is not reported for longer cracks, and clearly the accuracy of the stress intensity factor depends on the specific crack-face traction distribution.

The calculation of the SIF using the weight function method requires some care and attention to detail. The integration method used to solve Eq. (1) has a significant influence on the results, and needs to be selected based on the behavior of the stress and weight function fields along the crack line. Another important aspect to consider is the number of significant figures in the stress profile. The results from the weight function shown in Figure 7 were obtained using the input stress profile with full machine (15 digits) precision. Figure 13 shows the results of the weight function method using only six significant figures for the stress profile. It is clear that the results for long crack sizes are highly affected by the precision of the input stress profile, and effort should always be devoted to extract the highest number of significant figures available from the finite element model results.

The results in Figure 9 are worth further discussing. The relative difference in SIF between the equivalent model and the eigenstrain model is seen to be very small for the whole

range of crack sizes, which confirmed the principle of superposition. For the weight function, the results up to the first discontinuity point in the stress field (a/W = 0.25) agree very well with the results from the eigenstrain model, and the absolute value of the relative difference remains under 0.1%. After the first discontinuity point, this relative difference experiences a quick increase, and varies around 1%. It further increases after the second discontinuity point (a/W = 0.75), and reaches an absolute maximum of 4.2% at a/W = 0.9. It is important to point out that the weight function used in this paper was derived based on the assumption that the crack face displacement in plane stress can be represented by

$$u_r(a,x) = \frac{\sigma a/W\sqrt{1-x/a}}{\sqrt{2}\,E}\sum_{j=1}^{4} F_j(a/W)\left(1-\frac{x}{a}\right)^{j-1} \tag{10}$$

where $F_j(a/W)$ are functions of crack size that are determined by combinations of conditions on the crack behavior that depend on the type of crack (see [30]). The crack face displacement can be extracted from the eigenstrain FE model for selected crack sizes. Parker [33] showed that the crack face profile can also be calculated through an integration of the product of the weight function and the SIF, given by

$$u_r(a,x) = \frac{1}{\bar{E}}\int_x^a m(\alpha,x)\cdot K(\alpha)\,d\alpha \tag{11}$$

Comparing the crack face displacement profile obtained from the eigenstrain FE model and calculated using Eq. (11) is useful to evaluate the ability of the weight function to accurately predict crack face displacement in a discontinuous residual stress field. To illustrate, the crack face displacement was extracted from the eigenstrain FE model for two selected crack sizes (a/W = 0.25 and 0.60), and Eq. (11) was used to numerically calculate the displacement using Gauss-Kronrod quadrature [31]. The two crack sizes represent short and long cracks, and provide

information about the effect of crack size. The calculations used the SIF results from the FE model. Figure 14 shows the crack face displacement extracted from the eigenstrain FE model along with the calculated values using Eq. (11) as a function of normalized position along the crack face x/a. The results of Eq. (11) agree well with the displacement extracted from the eigenstrain FE model for both crack sizes, showing that the weight function can be used to accurately predict crack face displacement in a discontinuous residual stress field.

5. CONCLUSION

In this study, the objective was to provide a benchmark solution to a simple eigenstrain problem in a two-dimensional rectangular domain. The finite element method was used to model an edge cracked plate containing a known eigenstrain field, and obtain the stress in the uncracked body and the stress intensity factor as a function of crack size. A second finite element model was constructed to assess the validity of the principle of superposition, using crack face tractions, relative to the SIF calculation for this specific problem. The results from both FE models were found to be equivalent, which confirmed the validity of superposition and using only crack face traction to compute the SIF. In addition, results for the weight function method, using the formulation provided by Wu and Carlsson [15], were generally consistent with the finite element results, being in very good agreement up to a crack size of $a/W = 0.7$. At larger crack sizes, the weight function stress intensity factor results diverged from the FE results, but remained less than 4.2% for $a/W < 0.9$. The benchmark problem and solution are useful as a starting point for fracture mechanics calculations in residual stress bearing bodies using the eigenstrain approach, and lie at the intersection of linear elastic fracture mechanics and residual stress analysis.

REFERENCES

[1] McClung RC. A literature survey on the stability and significance of residual stresses during fatigue. Fatigue Fract Eng Mater Struct 2007;30:173–205. doi:10.1111/j.1460-2695.2007.01102.x.

[2] Luong H, Hill MR. The effects of laser peening and shot peening on high cycle fatigue in 7050-T7451 aluminum alloy. Mater Sci Eng A 2010;527:699–707. doi:http://dx.doi.org/10.1016/j.msea.2009.08.045.

[3] Rodopoulos CA, Romero JS, Curtis SA, de los Rios ER, Peyre P. Effect of controlled shot peening and laser shock peening on the fatigue performance of 2024-T351 aluminum alloy. J Mater Eng Perform 2003;12:414–9. doi:10.1361/105994903770342944.

[4] Clark G. Modelling Residual Stresses and Fatigue Crack Growth at Cold-Expanded Fastener Holes. Fatigue Fract Eng Mater Struct 1991;14:579–89. doi:10.1111/j.1460-2695.1991.tb00684.x.

[5] Hill MR. Determination of Residual Stress Based on the Estimation of Eigenstrain. Stanford University, 1996.

[6] Mura T. Micromechanics of defects in solids. Dordrecht, Netherlands: Martinus Nijhoff; 1987.

[7] DeWald AT, Hill MR. Eigenstrain-based model for prediction of laser peening residual stresses in arbitrary three-dimensional bodies Part 1: Model description. J Strain Anal Eng Des 2009;44:1–11. doi:10.1243/03093247jsa417.

[8] DeWald AT, Hill MR. Eigenstrain-based model for prediction of laser peening residual stresses in arbitrary three-dimensional bodies Part 2: Model verification. J Strain Anal Eng Des 2009;44:13–27. doi:10.1243/03093247jsa420.

[9] Coratella S, Sticchi M, Toparli MB, Fitzpatrick ME, Kashaev N. Application of the eigenstrain approach to predict the residual stress distribution in laser shock peened AA7050-T7451 samples. Surf Coatings Technol 2015;273:39–49. doi:http://dx.doi.org/10.1016/j.surfcoat.2015.03.026.

[10] Jun T-S, Korsunsky AM. Evaluation of residual stresses and strains using the Eigenstrain Reconstruction Method. Int J Solids Struct 2010;47:1678–86. doi:10.1016/j.ijsolstr.2010.03.002.

[11] Kartal ME, Kiwanuka R, Dunne FPE. Determination of sub-surface stresses at inclusions in single crystal superalloy using HR-EBSD, crystal plasticity and inverse eigenstrain analysis. Int J Solids Struct 2015;67-68:27–39. doi:10.1016/j.ijsolstr.2015.02.023.

[12] Achintha M, Nowell D. Eigenstrain modelling of residual stresses generated by laser shock peening. J Mater Process Technol 2011;211:1091–101. doi:10.1016/j.jmatprotec.2011.01.011.

[13] Hu Y, Grandhi R V. Efficient numerical prediction of residual stress and deformation for large-scale laser shock processing using the eigenstrain methodology. Surf Coatings Technol 2012;206:3374–85. doi:10.1016/j.surfcoat.2012.01.050.

[14] Bueckner HF. A novel principle for the computation of stress intensity factors. Zeitschrift fur Angewandte Mathemetik und Mechanik, vol. 50(9), p. 529–546; 1970.

[15] Wu X-R, Carlsson J. Weight functions and stress intensity factor solutions. Pergamon; 1991.

[16] Rice JR. Some remarks on elastic crack-tip stress fields. Int J Solids Struct 1972;8:751–8.

[17] Paris PC, McMeeking RM, Tada H. The weight function method for determining stress intensity factors. Cracks Fract 1976:471–89.

[18] Parker AP, Bowie OL. The weight function for various boundary condition problems. Eng Fract Mech 1983;18:473–7.

[19] Shen G, Glinka G. Weight functions for a surface semi-elliptical crack in a finite thickness plate. Theor Appl Fract Mech 1991;15:247–55. doi:http://dx.doi.org/10.1016/0167-8442(91)90023-D.

[20] Zheng XJ, Kiciak A, Glinka G. Weight functions and stress intensity factors for internal surface semi-elliptical crack in thick-walled cylinder. Eng Fract Mech 1997;58:207–21. doi:http://dx.doi.org/10.1016/S0013-7944(97)00083-0.

[21] Wong W, Hill MR. Superposition and Destructive Residual Stress Measurements. Exp Mech 2012;53:339–44. doi:10.1007/s11340-012-9636-y.

[22] Hill M, VanDalen J, VanDalen J. Evaluation of Residual Stress Corrections to Fracture Toughness Values. J ASTM Int 2008;5:1–11.

[23] ABAQUS/Standard, Version 6.11. Dassault Syst Simulia Corp, 2011:Providence, RI, USA.

[24] ABAQUS 6.11 Theory Manual. Dassault Syst Simulia Corp, 2011:Section 2.16.1, p. 1–5, Providence, RI, USA.

[25] Hou Y-C, Pan J. A fracture parameter for welded structures with residual stresses. Comput Mech 1998;22:281–8. doi:10.1007/s004660050360.

[26] Lei Y, O'Dowd NP, Webster GA. Fracture mechanics analysis of a crack in a residual stress field. Int J Fract 2000;106:195–216. doi:10.1023/A:1026574400858.

[27] Meith WA, Hill MR. Domain-independent values of the J-integral for cracks in three-dimensional residual stress bearing bodies. Eng Fract Mech 2002;69:1301–14. doi:http://dx.doi.org/10.1016/S0013-7944(02)00007-3.

[28] Anderson TL. Linear Elastic Fracture Mechanics. In: Fracture mechanics: fundamentals and applications. 3rd ed., CRC press; 2005, p. 54–7.

[29] Healy B, Gullerud AS, Koppenhoefer KC, Roy A, RoyChowdhury S, Petti J, et al. WARP3D: 3-D Dynamic Nonlinear Fracture Analysis of Solids Using Parallel Computers. Structural Research Series (SRS) 607, University of Illinois at Urbana-Champaign: 2015.

[30] Wu X-R, Carlsson J. Op Cit, ch. 6. 1991.

[31] Shampine LF. Vectorized adaptive quadrature in MATLAB. J Comput Appl Math

2008;211:131–40. doi:http://dx.doi.org/10.1016/j.cam.2006.11.021.

[32] ABAQUS 6.11 Release Notes. Dassault Syst Simulia Corp, 2011:Section 6.20, Providence, RI, USA.

[33] Parker AP. Stress intensity factors, crack profiles, and fatigue crack growth rates in residual stress fields. ASTM STP 1982;776:13–31.

TABLES

a/W	β_1	β_2	β_3	β_4	β_5
0.01	2.0000	0.9765	1.1420	-0.3504	-0.0912
0.05	2.0000	1.0927	1.1506	-0.3662	-0.0819
0.10	2.0000	1.4187	1.1377	-0.3549	-0.0763
0.15	2.0000	1.9056	1.1562	-0.3428	-0.0692
0.20	2.0000	2.5366	1.2379	-0.3475	-0.0561
0.25	2.0000	3.3108	1.4029	-0.3699	-0.0386
0.30	2.0000	4.2381	1.6796	-0.4095	-0.0188
0.35	2.0000	5.3370	2.1189	-0.4784	0.0045
0.40	2.0000	6.6359	2.8049	-0.6106	0.0394
0.45	2.0000	8.1770	3.8670	-0.8666	0.1021
0.50	2.0000	10.0222	5.4999	-1.3401	0.2178
0.55	2.0000	12.2627	8.0053	-2.1744	0.4247
0.60	2.0000	15.0359	11.8785	-3.6068	0.7858
0.65	2.0000	18.5559	17.9948	-6.0778	1.4211
0.70	2.0000	23.1752	28.0304	-10.4966	2.5867
0.75	2.0000	29.5188	45.5064	-18.9278	4.8833
0.80	2.0000	38.8127	78.7526	-36.5960	9.8713
0.85	2.0000	53.8458	151.2114	-79.0143	22.2693
0.90	2.0000	82.6872	350.9948	-207.0899	60.8586

Table 1 – β_i for a single edge crack in a finite width plate.

FIGURES

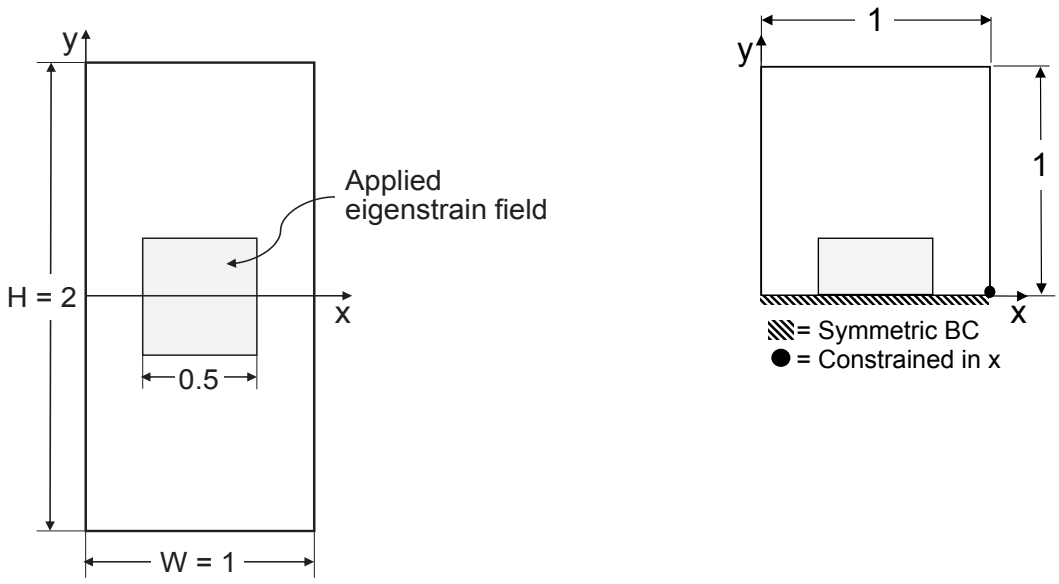

(a) (b)

Figure 1 – (a) Problem geometry and eigenstrain application area, (b) half-model with boundary conditions

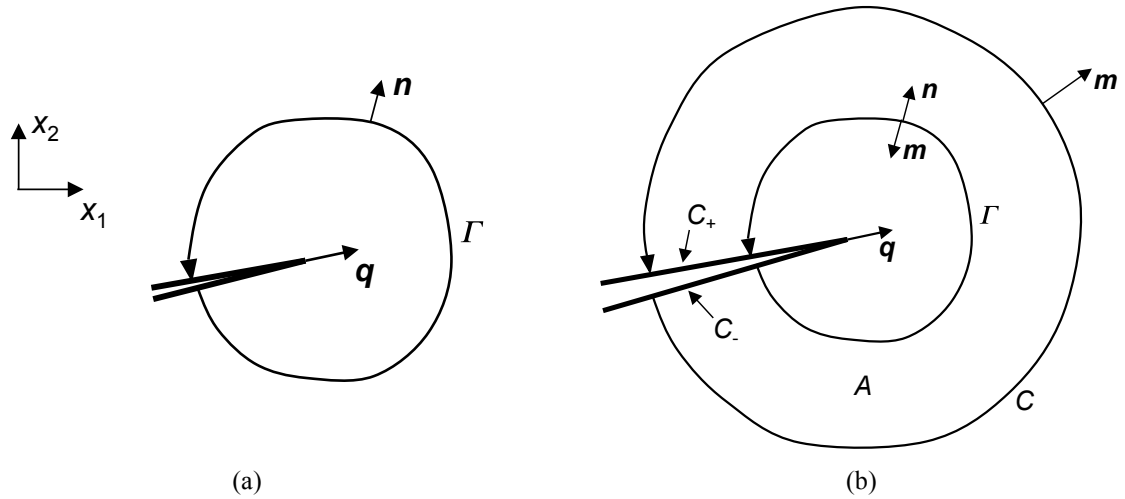

(a) (b)

Figure 2 – (a) Parameters for fracture mechanics contour integral, (b) parameters for domain integral (adapted from [24]*)*

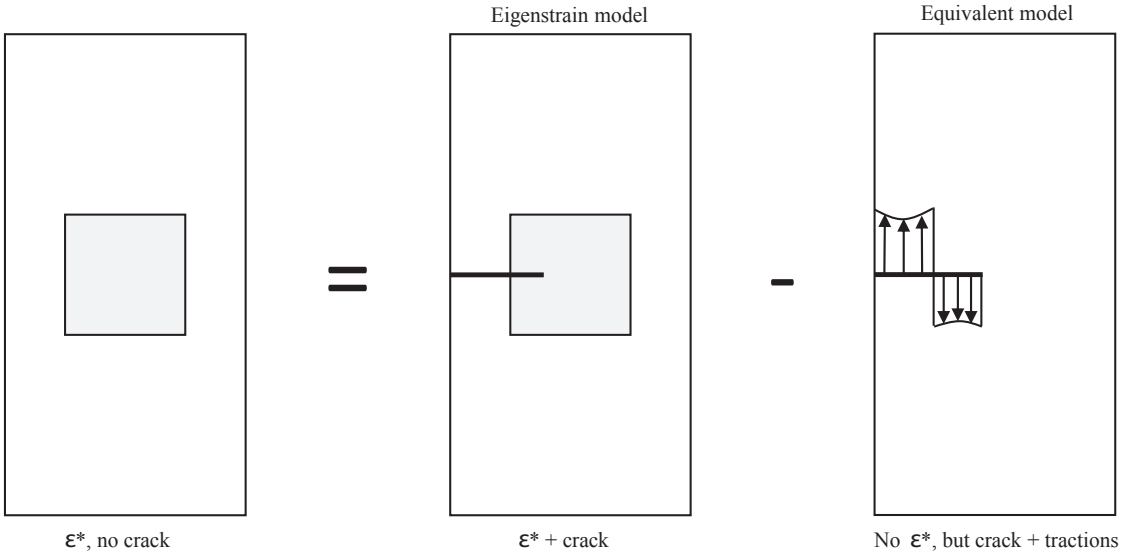

Figure 3 – Applied principle of superposition. (a) uncracked plate with eigenstrain field; (b) plate with eigenstrain field and edge crack; (c) plate with edge crack and crack face stress field

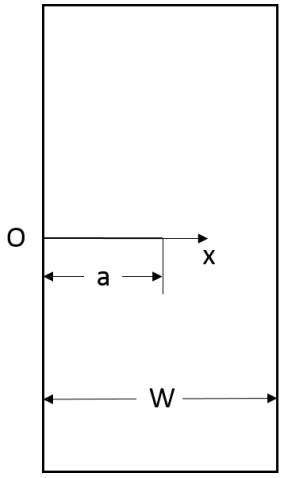

Figure 4 – Edge crack in a finite width plate (adapted from [15]*)*

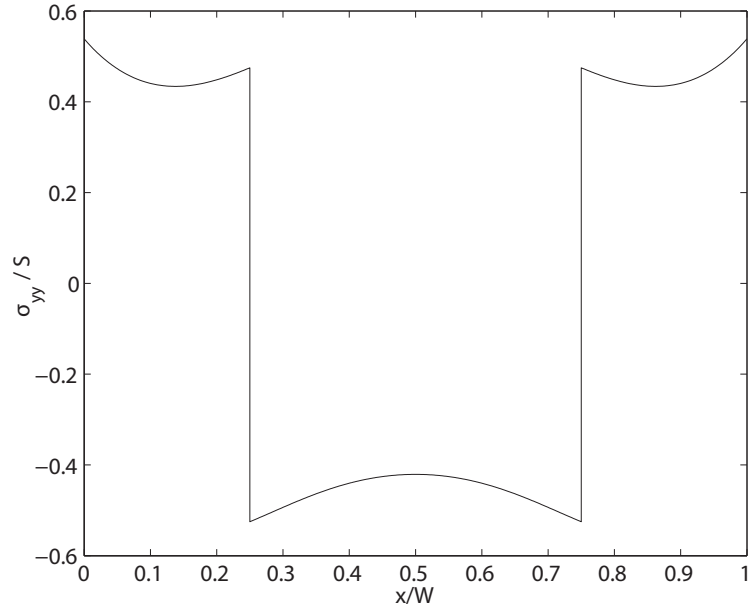

Figure 5 – Residual stress at the crack line (σ_{yy})

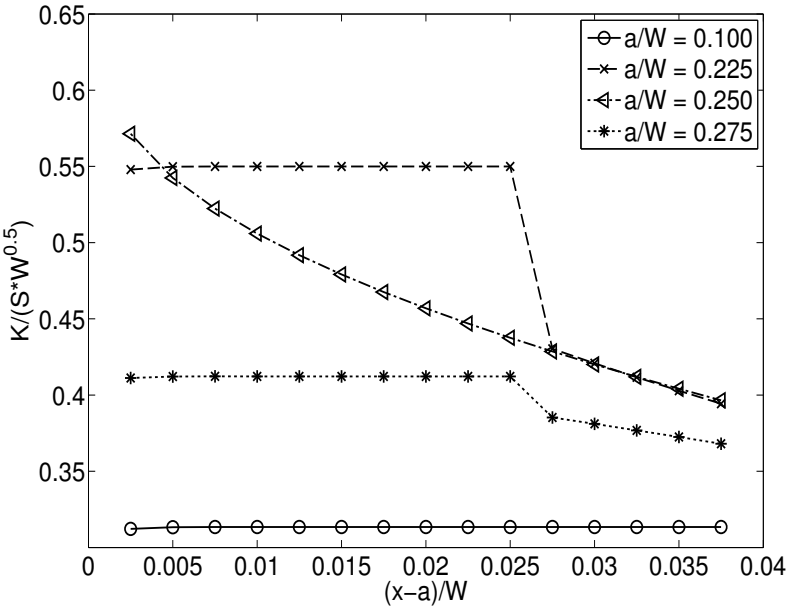

Figure 6 – Normalized SIF as a function of domain size from eigenstrain FE model

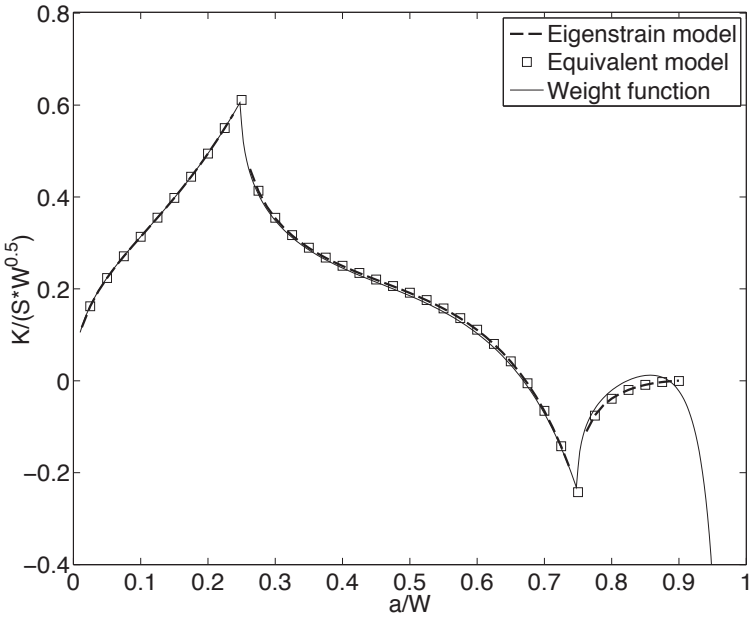

Figure 7 – Normalized SIF as a function of crack size from weight function and finite element models

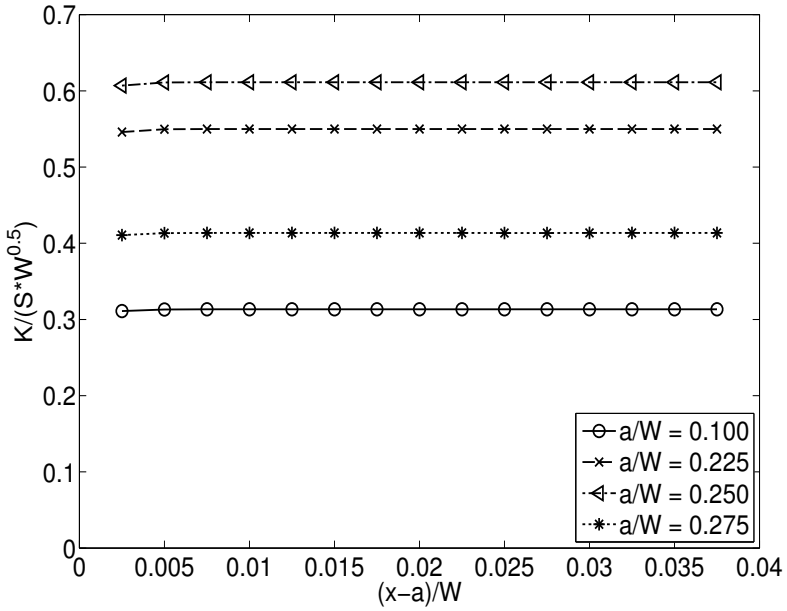

Figure 8 *– Normalized SIF as a function of domain size from equivalent FE model*

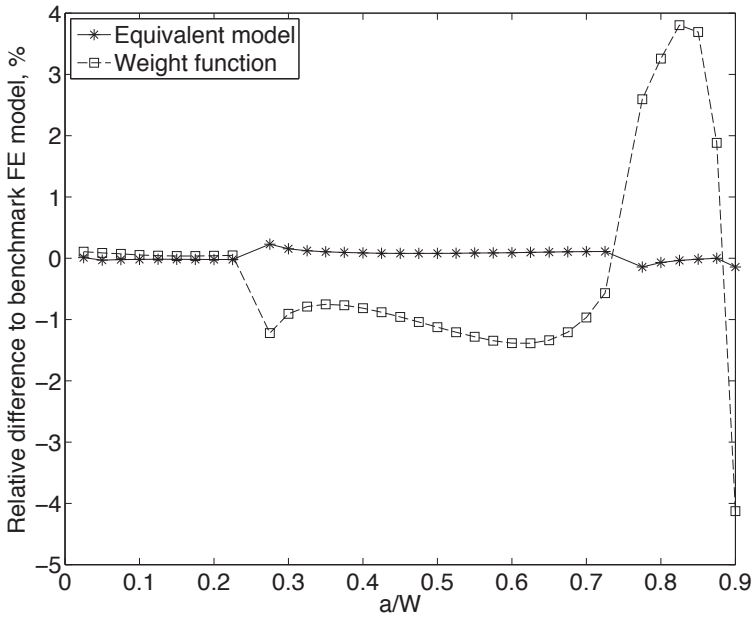

Figure 9 – Relative difference (in SIF) to eigenstrain FE model (benchmark)

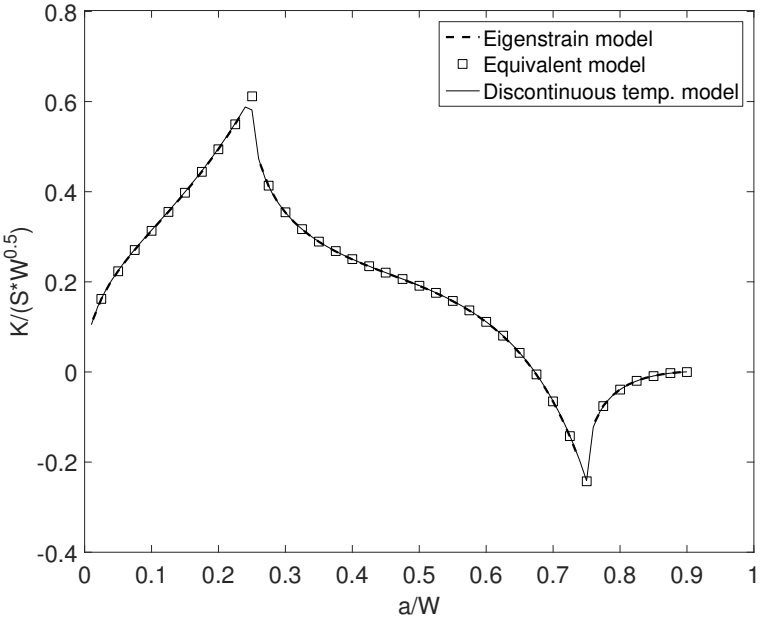

Figure 10 – Normalized SIF as a function of crack size from discontinuous temperature FE model and previous FE models

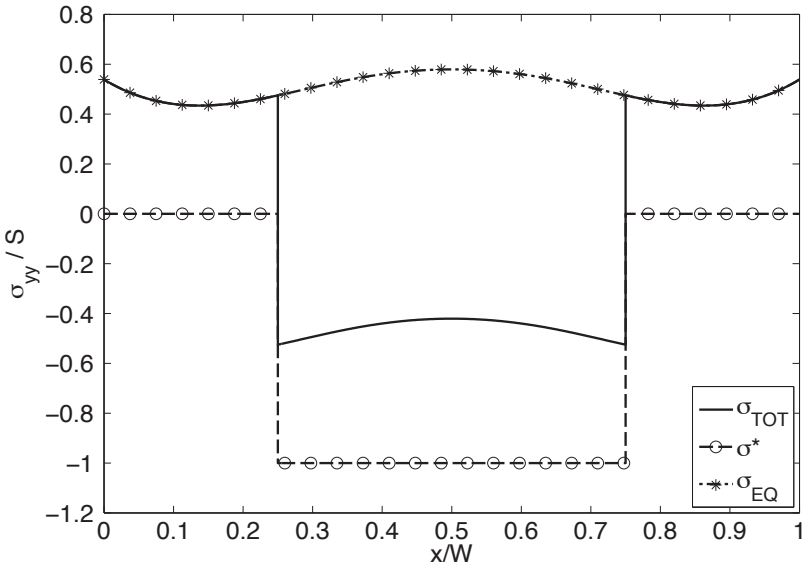

Figure 11 – Superposition of the residual stress distribution

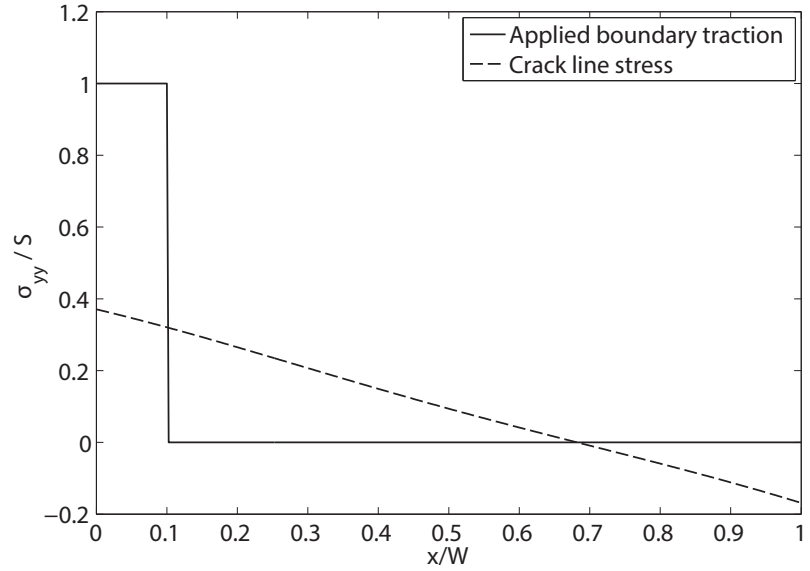

Figure 12 – Applied boundary traction and resulting crack line stress

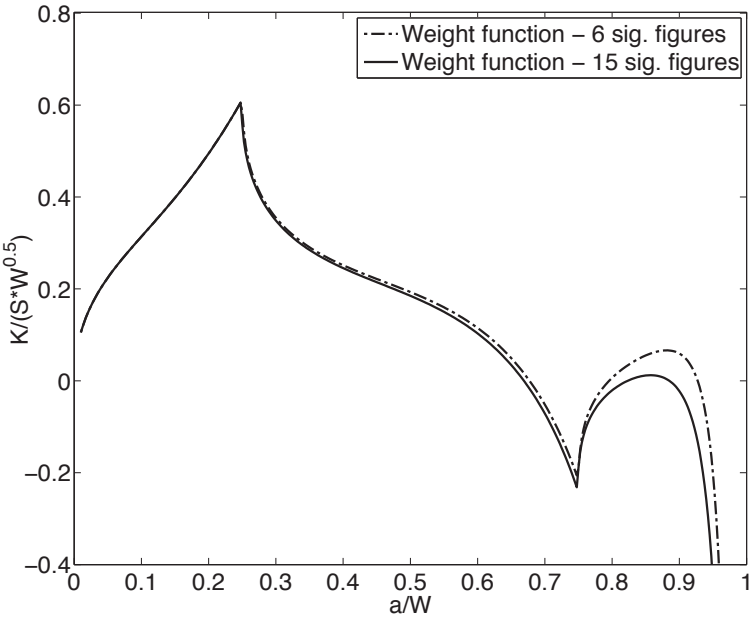

Figure 13 – Effect of number of significant figures of input stress in the SIF from weight function

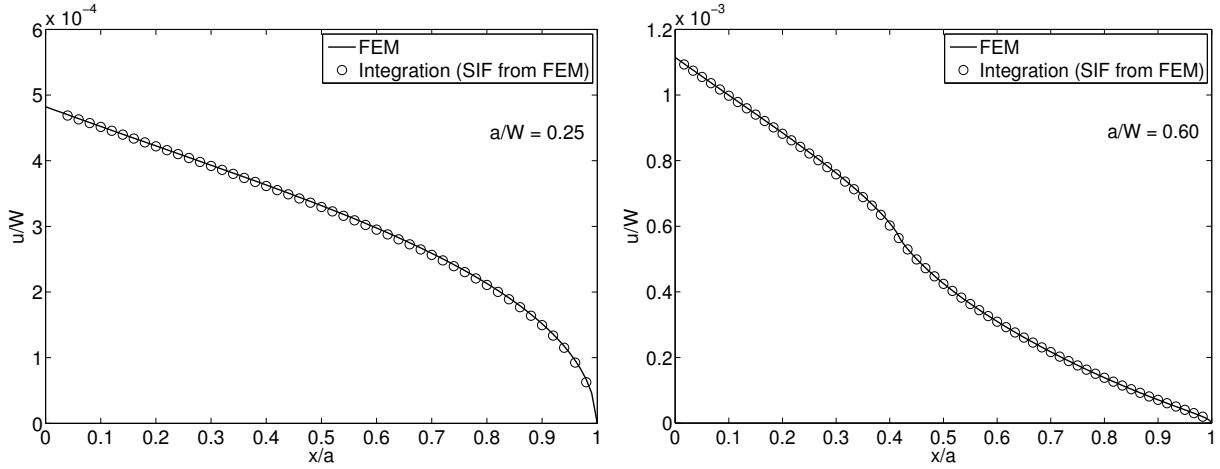

(a) (b)

Figure 14 – Crack face displacement for (a) a/W = 0.25, (b) a/W = 0.6